Doped V_2O_5-Based Cathode Materials: Where Does the Doping Metal Go? An X-ray Absorption Spectroscopy Study

Marco Giorgetti* and Mario Berrettoni

Department of Physical and Inorganic Chemistry, University of Bologna and Unità di Ricerca INSTM di Bologna, Viale del Risorgimento 4, 40136 Bologna, Italy

William H. Smyrl*

Department of Chemical Engineering and Materials Science, University of Minnesota, 421 Washington Avenue S.E., Minneapolis, Minnesota 55455

Received July 18, 2007. Revised Manuscript Received September 24, 2007

X-ray absorption spectroscopy (XAS) has been used to probe the local structure of doped vanadium pentoxide materials prepared through sol–gel processes. The doped samples have been analyzed at the vanadium K-edge as well as at the doping metal K-edge (copper and zinc). The presence of two metal sites gives two independent absorption signals, even if we are investigating the same compound; for this reason the reliability of the analysis is enhanced. The strategy in determining the local structure will be discussed. The local structural modifications resulting from low to high doping concentration in the best performing copper-doped V_2O_5 aerogel like material is reported. Similar measurements were done using zinc as doping metal, in both aerogel-like and xerogel form. The EXAFS analysis shows that the vanadium atomic environment is not altered by the doping metal insertion and that the doping metals (Cu and Zn) are found to be in the same site. Copper and zinc are 4-fold coordinated by almost coplanar oxygens in both xerogel and aerogel-like oxide hosts. The use of the metal–metal interaction while analyzing data concerning sample of high doping level played a key role in the determination of the preferred metal sites.

Introduction

The preparation of vanadium pentoxide via sol–gel processes has been extensively reported, and comprehensive reviews are available.[1,2] This class of materials shows exceptional stability, intercalation capacity, and reversibility, allowing applications as intercalation hosts for lithium ions. The electrochemical properties of vanadium oxide electrodes prepared by sol–gel processes have been shown to depend on the structural and morphological characteristics, which are quite sensitive to the preparation method. Following this synthesis route, a number of pillared and pristine nanocomposites of vanadium pentoxide have been studied and characterized.[3,4] The materials are amorphous and have intercalation capacity as high as 650 Ah/kg with corresponding specific energies exceeding 1600 Wh/kg. Because of the amorphous state, structural information is likely to be obtained using the X-ray absorption spectroscopy technique (XAS)[5] as a local structural probe, as demonstrated by typical application in the field of disordered, amorphous, crystalline,[6] and biological materials[7] and to solutions[8] as well.

Previous studies by XAS techniques on the V_2O_5-based compounds allowed us to determine fundamental structural information on a wide variety of native and pillared nanocomposites[9–15] using both ex-situ and in-situ techniques. Soft X-ray absorption spectroscopic studies on vanadium oxide nanotubes have also been reported.[16]

To enhance the rate of insertion, the electronic conductivity of amorphous V_2O_5 was increased by doping with Ag, Cu, and Zn: an increase of the conductivity by more than 3 orders

* To whom correspondence should be addressed: e-mail marco.giorgetti@unibo.it, Ph +39 051 209 3666, Fax +39 051 209 3690; e-mail smyrl001@umn.edu.

(1) Livage, J. *Coord. Chem. Rev.* **1998**, *178–180*, 999.
(2) Chirayil, T.; Zavalij, P. Y.; Whittingham, M. S. *Chem. Mater.* **1998**, *10*, 2629.
(3) Le, D. B.; Passerini, S.; Tipton, A. L.; Owens, B. B.; Smyrl, W. H. *J. Electrochem. Soc.* **1995**, *142*, L102.
(4) Coustier, F.; Hill, J.; Owens, B. B.; Passerini, S.; Smyrl, W. H. *J. Electrochem. Soc.* **1999**, *146*, 1355 and references therein.
(5) Rehr, J. J.; Albers, R. C. *Rev. Mod. Phys.* **2000**, *72*, 621.
(6) Filipponi, A. *J. Phys.: Condens. Matter* **2001**, *13*, R23.
(7) Giorgetti, M.; Ascone, I.; Berrettoni, M.; Conti, P.; Zamponi, S.; Marassi, R. *J. Biol. Inorg. Chem.* **2000**, *5*, 156.
(8) D'Angelo, P.; Benfatto, M.; Della Longa, S.; Pavel, N. V. *Phys. Rev. B* **2002**, *66*, 064209.
(9) Giorgetti, M.; Passerini, S.; Smyrl, W. H.; Berrettoni, M. *Inorg. Chem.* **2000**, *39*, 1514.
(10) Giorgetti, M.; Mukerjee, S.; Passerini, S.; McBreen, J.; Smyrl, W. H. *J. Electrochem. Soc.* **2001**, *148*, A768.
(11) Giorgetti, M.; Passerini, S.; Smyrl, W. H.; Berrettoni, M. *Chem. Mater.* **1999**, *11*, 2257.
(12) Frabetti, E.; Deluga, G. A.; Smyrl, W. H.; Giorgetti, M.; Berrettoni, M. *J. Phys. Chem. B* **2004**, *108*, 3765.
(13) Giorgetti, M.; Passerini, S.; Smyrl, W. H.; Muckerjee, S.; Yang, X. Q.; McBreen, J. *J. Electrochem. Soc.* **1999**, *146*, 2387.
(14) Giorgetti, M.; Passerini, S.; Berrettoni, M.; Smyrl, W. H. *J. Synchrotron Radiat.* **1999**, *6*, 743.
(15) Giorgetti, M.; Berrettoni, M.; Passerini, S.; Smyrl, W. H. *Electrochim. Acta* **2002**, *47*, 3163.
(16) Nordlinder, S.; Augustsson, A.; Schmitt, T.; Guo, J.; Duda, L. C.; Nordgren, J.; Gustafsson, T.; Edstrom, K. *Chem. Mater.* **2003**, *15*, 3227.

10.1021/cm701910c CCC: $37.00
Published on Web 10/31/2007

Table 1. List of the Investigated Compounds $M_xV_2O_5$ with Actual Element Concentration (ICP-MS)

sample	$x \sim 0.25$	$x \sim 0.50$	$x \sim 0.75$	$x \sim 1.00$
Cu ARG-like V_2O_5	**a** (0.26)	**b** (0.51)	**c** (0.37)	**d** (1.03)
Zn ARG-like V_2O_5	**e** (0.24)			**f** (0.98)
Cu XRG V_2O_5		**g** (0.52)		**h** (1.01)
Zn XRG V_2O_5			**i** (0.76)	**l** (1.02)

of magnitude was found. Subsequent intercalation of Li^+ into the doped materials was facile and highly reversible. The nanocomposites of the Cu-doped sample were shown to support high rates for lithium intercalation. A previous paper based on a XAS study on the copper- and zinc-doped samples (with $x = 0.25$) gave details about the site where the doping metals are located, also demonstrating its equivalency; i.e., copper and zinc go to the same site.[12] Also, an in-situ XAS experiment[10] showed that the copper ion was reduced to the metallic state during lithium insertion and reoxidized, returning to the same site in the lattice upon lithium release.

This paper describes the identification of the metal sites occupied by the copper and zinc, as a function of the doping level, in gel-based V_2O_5. Xerogel (XRG) and aerogel-like (ARG-like) materials were investigated. To study the structural sites of the polyvalent ions, EXAFS (extended X-ray absorption fine structure) spectra has been recorded at the zinc, copper, and vanadium K-edge in a series of aerogel-like and xerogel V_2O_5-doped materials. The paper highlights the ability of the XAS technique to determine the preferred site of the doping metal, with a straightforward application of the multiple scattering (MS) formalism in the XAS data analysis.

Experimental Section

Synthesis. Vanadium pentoxide hydrogels were synthesized from sodium metavanadate by an ion exchange process.[3] The copper- and zinc-doped V_2O_5 XRG materials were prepared following ref 10. The copper- and zinc-doped V_2O_5 ARG-like were prepared as described earlier by Coustier et al.,[4] except for some slight modifications adopted to facilitate the gel preparation with a high metal concentration. Briefly, the doping was performed by mixing the selected stoichiometric amount of copper or zinc powder (ALFA 99.997% purity) with the V_2O_5 hydrogel. After the reaction was complete, the samples were dried under vacuum for several days. Table 1 summarizes the samples under investigation prepared following the above-mentioned procedures. X-ray powder diffraction of the investigated samples indicated an amorphous state for all samples (see Supporting Imformation). The absence of peaks associated with metallic copper or zinc clearly indicated that the reaction was complete. Only sample **f** was found to be contaminated with Zn metal, and it will not considered further. Sample **c** analysis indicates that the copper has been inserted with poor efficiency ($x \sim 0.37$ instead of the stoichiometric 0.75), and in fact the XANES at the copper K-edge (see Figure 4a) are similar to that of sample **a**.

XAS Data Collection. Samples for the XAS experiments were mixed with boron nitride and then were pressed as pellets (3 tons). X-ray absorption experiments were performed at the Synchrotron Radiation Source (SRS) at Daresbury Laboratory, Warrington, England, using the beamline 7.1. The storage ring operates at 1.6 GeV and a typical current of 240 mA. Internal references for energy calibration were used for vanadium, zinc, and copper at each scan.

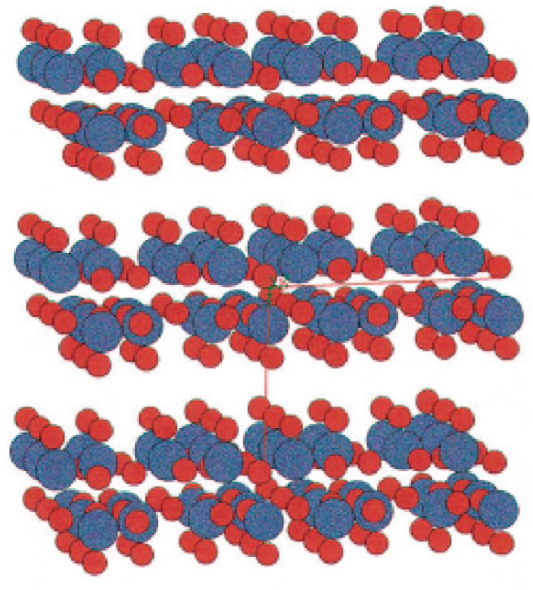

Figure 1. Bilayer structure of the gels. Each V_2O_5 layer is facing another layer with a distance of 2.8 Å. The interplanar distance (or interlayer spacing) is enough to accommodate the guest species such as cations. The preferred cation "site" could be close to a single bilayer as well as in the space between two bilayers.

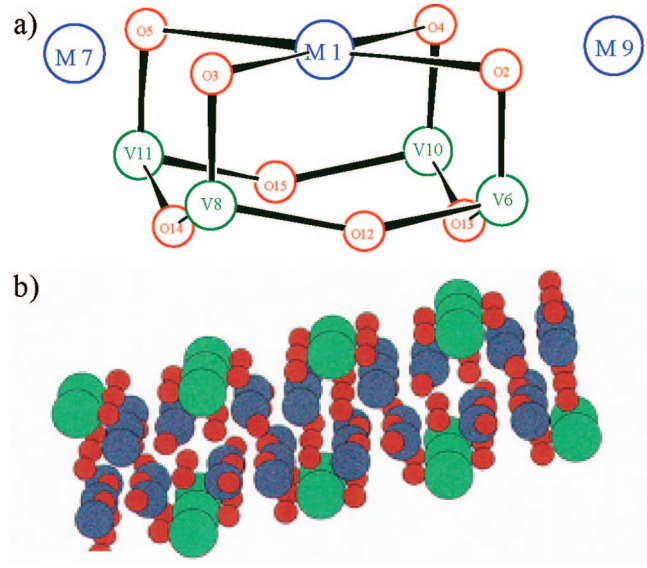

Figure 2. (a) Proposed "ball and stick" structure of the zinc site in anhydrous $M_xV_2O_5$ samples. M is 4-fold-coordinated by apical oxygens of close VO_6 units. For the sake of clarity, the interaction between two different metal atoms is also indicated. (b) Bilayer structure of the $M_1V_2O_5$ gels where M atoms interact within a single bilayer.

This allows for a continuous monitoring of the energy during consecutive scans. No energy drifts of the monochromator were observed during the experiments. Data were acquired in transmission mode. The ionization chamber was filled with an Ar/He gas mixture. Harmonics were rejected by detuning (80%). X-ray absorption spectra (XAS) were collected from 200 eV before the edge up to $k = 15$ every 0.03 k with a 3 s integration time (zinc and copper K-edge) and up to $k = 12$ every 0.03 k for 3 s (vanadium K-edge).

XAS Data Analysis. XANES spectra were normalized to an edge jump of unity taking into account the atomic background after the edge as revealed from the EXAFS analysis. A prior removal of the background absorption was done by subtraction of a linear function extrapolated from the pre-edge region. The EXAFS analysis has

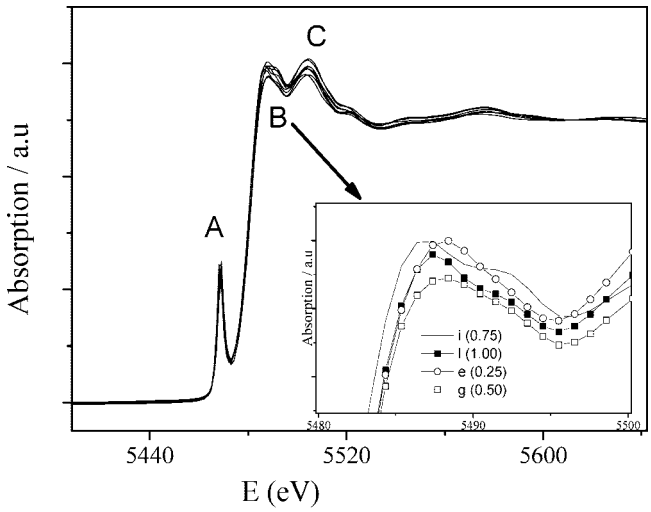

Figure 3. XANES spectra at the vanadium K-edge (5565 eV) of the investigated samples.

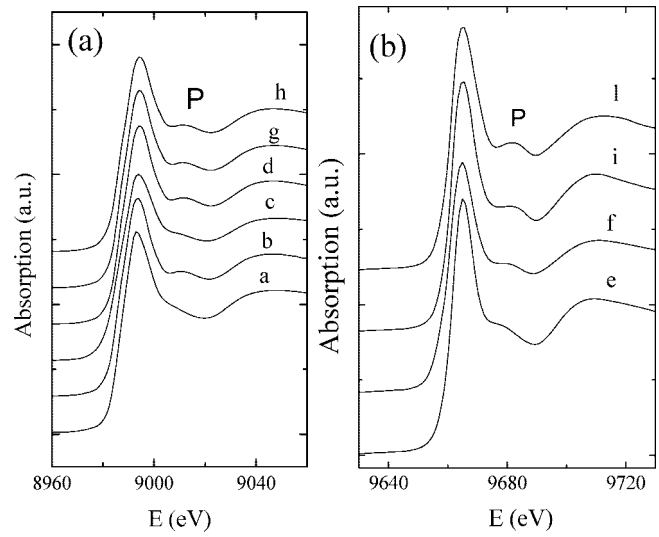

Figure 4. XANES spectra at the Cu K-edge (panel a) and Zn K-edge (panel b) of the investigated samples.

been performed by using the GNXAS package[17,18] which takes into account multiple scattering (MS) theory. The method is based on the decomposition of the EXAFS signals into a sum of several contributions, the *n*-body terms. It allows the direct comparison of the raw experimental data with a model theoretical signal. The procedure avoids any filtering of the data and allows a statistical analysis of the results. The theoretical signal is calculated ab initio and contains the relevant two-body $\gamma^{(2)}$ and the three-body $\gamma^{(3)}$ multiple scattering (MS) terms. The contribution from four-body $\gamma^{(4)}$ terms[19] has been checked out, but it was found negligible. The two-body terms are associated with pairs of atoms and probe their distances and variances. The three-body terms are associated with triplets of atoms and probe angles and bond–bond and bond–angle correlations. If useful, a single effective MS signal $\eta^{(3)}$ that includes both $\gamma^{(2)}$ and the $\gamma^{(3)}$ contributions can be used for the shells beyond the second one by using the same three-atom coordinates for both the two-atom and the three-atom contributions. The full definition of the parameters associated with the triplet of atoms is found in ref 18. Data analysis is performed by minimizing a χ^2-like function that compares the theoretical model to the experimental signal.

The phase shifts for the photoabsorber and backscatterer atoms were calculated ab initio starting from the structural model that was discussed in ref 12. They were calculated according to the muffin-tin approximation. The Hedin–Lundqvist complex potential[20] was used for the exchange-correlation potential of the excited state. Hereafter in the analysis, the starting signals have been successively recalculated to account for any important structural variation from the starting model. In fact, when a deviation of more that 10% of a selected structural parameter (e.g., atomic distance or angle) occurred with respect to the crystallographic values, the corresponding theoretical signal has been recalculated before being used in the fitting procedure.

The core hole lifetime, Γ_c, was fixed to the tabulated value[21] and included in the phase shift calculation. The experimental resolution used in the fitting analysis was about 2 eV, in agreement with the stated value for the beamline used. The value of S_0^2 has been found to be between 0.78 and 0.91 for the vanadium, copper, and zinc K-edge. The relevant E_0's values are found to be displaced by several electronvolts with respect to the edge inflection point.

In order to evaluate the effect of the structural disorder, the simulation was done by considering a non-Gaussian type of pair distribution functions. In fact, because of the amorphous nature of the compound, a more flexible model that replaces the simple Gaussian function might be expected to be required. The gamma-like (Γ) distribution has been used here[22,23] and proven to be very useful in previous studied systems.[24–26] The function depends on three parameters: the average bond distance, the bond variance, and the asymmetry coefficient (skewness) β defined as K_3/σ^3, where K_3 is the third cumulant of the distribution. The full definition of the function is described in refs 18 and 23.

Results and Discussion

The local and long-range structure of V_2O_5 gel is described[9,15,27] by almost perfect pairs of single V_2O_5layers made of square-pyramidal VO_5 units facing each other (i.e., the typical bilayer), where the interlayer distance is found to be affected by the method of preparation (d = 8.8 Å for xerogel and d =12.5 Å for aerogel); both distances are different from the crystalline V_2O_5 distance (4.4 Å). The structure is shown in Figure 1. The peculiar V_2O_5 gel structure offers the possibility of intercalating several ions, and the V_2O_5 gels may act as a universal host.[28] Structurally speaking, there are two possible sites where an ion (guest) could be placed into the host: between two bilayers or close to a single one. For instance, the zinc atom is found between two layers in $Zn_{0.25}V_2O_5$ crystalline hydrated samples

(17) Filipponi, A.; Di Cicco, A.; Natoli, C. R. *Phys. Rev. B* **1995**, *52*, 15122.
(18) Filipponi, A.; Di Cicco, A. *Phys. Rev. B* **1995**, *52*, 15135.
(19) Giorgetti, M.; Berrettoni, M.; Filipponi, A.; Kulesza, P. J.; Marassi, R. *Chem. Phys. Lett.* **1997**, *275*, 108.
(20) Hedin, L.; Lundvquist, B. I. *J. Phys. C* **1971**, *4*, 2064.
(21) Krause, M.; Oliver, J. H. *J. Phys. Chem. Ref. Data* **1979**, *8*, 329.
(22) Filipponi, A. *J. Phys.: Condens. Matter* **1994**, *6*, 8415.
(23) Filipponi, A.; Di Cicco, A. *Task Q.* **2000**, *4*, 575.
(24) Dalba, G.; Fornasini, P.; Grisenti, R.; Rocca, F. *J. Non-Cryst. Solids* **2004**, *345&346*, 7.
(25) D'Angelo, P.; Di Nola, A.; Filippini, A.; Pavel, N. V.; Roccatano, D. *J. Chem. Phys.* **1994**, *100*, 985.
(26) Giorgetti, M.; Berrettoni, M.; Scaccia, S.; Passerini, S. *Inorg. Chem.* **2006**, *45*, 2750.
(27) Petkov, V.; Trikalitis, P. N.; Bozin, E. S.; Billinge, S. J. L.; Vogt, T.; Kanatzidis, M. G. *J. Am. Chem. Soc.* **2002**, *124*, 10157.
(28) Le, D. B.; Passerini, S.; Coustier, F.; Guo, J.; Soderstrom, T.; Owens, B. B.; Smyrl, W. H. *Chem. Mater.* **1998**, *10*, 682.

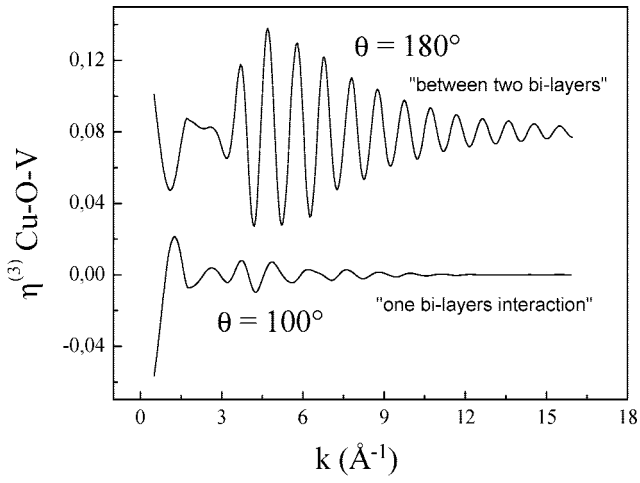

Figure 5. Theoretical $\eta^{(3)}$ signal associated to the M–O–V triplet computed for linear (180°) and coplanar (100°) geometries. The calculation has been done considering Cu as doping metal. The degeneracy of the path is 2, and the signal includes both two-body $\gamma^{(2)}$ Cu–V and three-body $\gamma^{(3)}$ Cu–O–V multiple scattering signals.

obtained by hydrothermal synthesis.[29] On the contrary, it was demonstrated that chemically inserted zinc in $Zn_xV_2O_5$ aerogel interacts with a single bilayer[11] where the zinc is 4-coordinated by the apical oxygens of four VO_6 octaedra. These oxygens belong to the same V_2O_5 bilayer, and the zinc site is in the quasi-coplanar position with them.

This local atomic arrangement is depicted in Figure 2, where the metal (M) interacts with a single bilayer. The number of such a sites would be filled as the stoichiometric coefficient x in the general formula $M_xV_2O_5$ approaches one. Figure 2b shows the proposed structure of $M_{1.0}V_2O_5$ displaying the interaction of a large number of metal atoms within a single V_2O_5 bilayer. In this context, the present study focuses mainly on the structural characteristic of samples with a high level of the doping metal, i.e., the compounds **d**, **h**, and **l** of Table 1.

Structural studies of the intercalation sites in the doped V_2O_5 materials were performed using X-ray absorption spectroscopy at the copper, zinc, and vanadium K-edges. It has already been demonstrated that the simultaneous presence of zinc or copper with the vanadium is very useful[12] because it makes available a second photoabsorber atom to be probed by XAS whereby one uses both the metal and vanadium K-edges, providing complementary structural information. Data analysis at the three different K-edges is presented.

XANES. The intrinsic first-shell symmetry is distorted in the VO_6 pseudo-octahedron in V_2O_5-based material, and the X-ray near-edge structure (XANES) at the vanadium K-edge has become a very useful tool for investigating its electronic and geometric structure. Indeed, the vanadium K-edge is very sensitive to the local symmetry of the vanadium as well as to the associated charge of the metal itself. Several comprehensive papers are available regarding this aspect.[13,30,31]

Figure 3 shows the XANES region of the V K-edge for the investigated compounds. All spectra showed a pre-edge peak A that is well-known to be due to a formally forbidden 1s–3d electronic transition[13] which is dipole allowed if the full local O_h symmetry is decreased. Also, the main peak B and the peak at about 5505 eV are resonances of the photoelectron and are due to transitions from core levels to nonbinding levels in the continuum. The low energy of the emitted photoelectron allows strong multiple scattering effects that were shown to have an angular dependence.[32] At a first glance, none of the features changed in intensity or in energy with different zinc or copper intercalation level, therefore indicating a substantial stability of the vanadium oxidation state as well as of the local vanadium environment. Data also show that there is no significant difference in the vanadium atomic environment when the nature of the doping metal is changed or when the same material made by two different routes of synthesis is compared. The only difference, apart from a slight change in the energy position (for instance of the pre-edge peak A, of about 0.5 eV), is visible on the feature B, where high metal content samples causes splitting onto two features. This is clear from the inset of the figure which displays a magnification of the edge region for samples **i**, **l**, **e**, and **g**.

Figure 4 shows the XANES curves recorded at the Cu (panel a) and Zn K-edge (panel b) of the copper- and zinc-doped V_2O_5 samples. At a first glance, each series of spectra of both panels shows a similar curve shape; i.e., copper or zinc seems to interact with the V_2O_5 bilayer comparably, as the similarity of the two elements in the periodic table may suggest. Also, no shift of the edge, within the experimental resolution, is detected. Both spectra series are characterized by two main features, the main edge and the feature P, that straighten as the metal level content increases. This is clearly apparent from both Cu and Zn K-edge spectra. This feature has been observed in binuclear zinc clusters with square-planar geometry[33] and in $ZnFe_2O_4$ spinel with the Zn^{2+} ions to be in tetrahedral site[34] . Eventually, the almost constant value of the edge position indicates a relatively constant value for the effective charge of the inserted copper or zinc ions for all compounds.

EXAFS at the Copper and Zinc K-Edges. In order to gain a deeper insight into the metal–V_2O_5 interaction and to fully investigate the sites where the metal ions are located, the extended range of the X-ray absorption spectrum of the samples indicated in Table 1 was analyzed. EXAFS analysis was done using a multiple scattering (MS) approach that has been proved to be very efficient in several applications[26,35] and that has become very useful when particular atomic geometries are involved.

Here, the specific structural parameter playing a key role is the value of the angle M–O–V (shown for instance in

(29) Oka, Y.; Tamada, O.; Yao, T.; Yamamoto, N. *J. Solid State Chem.* **1996**, *126*, 65.
(30) Wong, J.; Lytle, F. W.; Messmer, R. P.; Maylotte, D. H. *Phys. Rev. B* **1984**, *30*, 5596.
(31) Giuli, G.; Paris, E.; Mungall, J.; Romano, C.; Dingwell, D. *Am. Mineral.* **2004**, *89*, 1640.
(32) Stizza, S.; Mancini, G.; Benfatto, M.; Natoli, C. R.; Garcia, J.; Bianconi, A. *Phys. Rev. B* **1989**, *40*, 12229.
(33) Ascone, I.; Lenouvel, F.; Sequeval, D.; Dexpert, H.; Felenbok, B. *Biochim. Biophys. Acta* **1997**, *1343*, 211.
(34) Steward, S. J.; Figueroa, S. J. A.; Ramallo Lopez, J. M.; Marchetti, S. G.; Bengoa, J. F.; Prado, R. J.; Requejo, F. G. *Phys. Rev. B* **2007**, *75*, 073408.
(35) Hayakawa, K.; Hatada, K.; Angelo, P. D.; Della Longa, S.; Natoli, C. R.; Benfatto, M. *J. Am. Chem. Soc.* **2004**, *126*, 15618.

Table 2. EXAFS Best-Fitting Results of $Cu_xV_2O_5$ Materials[a]

bond length [degeneracy] Debye–Waller	$x = 0.25$ Cu arg-like	$x = 0.50$ Cu arg-like	$x = 1.00$ Cu arg-like	$x = 0.50$ Cu xerogel	$x = 1.00$ Cu xerogel
Cu–O/Å [4]	1.970(6)	1.954(6)	1.954(6)	1.953(6)	1.956(8)
σ^2/Å^2	0.004(1)	0.004(1)	0.006(2)	0.005(2)	0.005(2)
β	0.4(1)	0.5(2)	0.4(1)	0	0
Cu–O/ Å [4]	2.280(8)	2.30(1)	2.34(1)	2.33(2)	2.30(2)
σ^2/Å^2	0.029(1)	0.029(3)	0.026(3)	0.026(7)	0.028(10)
Cu–Cu/Å	*3.10(8)*	3.01(1)	3.01(1)	3.01(1)	3.02(1)
σ^2/Å^2	*0.02(1)*	0.007(3)	0.008(2)	0.007(3)	0.008(4)
CN	*0.4(3)*	2.5(5)	2.5(5)	2.6(4)	2.7(4)
V–O apical/Å [4]	1.67(2)	1.59(1)	1.59(2)	1.61(2)	1.59(2)
σ^2/Å^2	0.008(6)	0.010(2)	0.014(6)	0.009(3)	0.005
Cu--V/Å[b]	2.81[b]	2.79[b]	2.83[b]	2.80[b]	2.81[b]
Cu–O–V/deg	101(1)	104(1)	105(3)	105(2)	104(2)
$\sigma^2\theta$/deg^2	73(20)	76(18)	68(15)	68(20)	75(40)

[a] The estimated parameter errors are indicated in parentheses. [b] Data obtained from the three-body configuration (using angle M–O–V and distances V–O).

Table 3. EXAFS Best-Fitting Results of $Zn_xV_2O_5$ Materials[a]

bond length [degeneracy] Debye–Waller	$x = 0.25$ Zn arg-like	$x = 0.75$ Zn xerogel	$x = 1.00$ Zn xerogel
Zn–O/Å [4]	2.069(3)	2.059(2)	2.048(5)
σ^2/Å^2	0.008(1)	0.009(1)	0.012(8)
β	0.10(5)	0.0	0.27(4)
Zn–O/ Å [4	2.30(1)	2.301(7)	2.304(8)
σ^2/Å^2	0.04(2)	0.026(3)	0.039(3)
Zn–Zn/Å	*2.90(8)*	3.09(1)	3.09(1)
σ^2/Å^2	*0.02(1)*	0.007	0.011
CN	*0.5(3)*	2.2(4)	2.9(5)
V–O apical/Å [4]	1.69(1)	1.63(1)	1.63(3)
σ^2/Å^2	0.015(7)	0.012(2)	0.013(5)
Zn--V/Å[b]	2.80[b]	2.77[b]	2.88[b]
Zn–O–V/deg [4]	95(1)	97(1)	103(2)
$\sigma^2\theta$/deg^2	50(10)	46(10)	36(9)

[a] The estimated parameter errors are indicated in parentheses. [b] Data obtained from the three body configuration (using angle M–O–V and distances V–O).

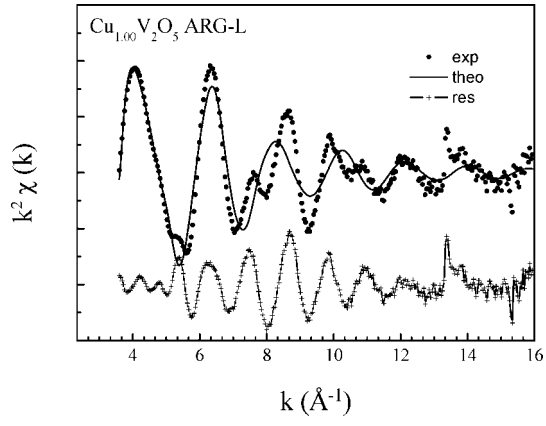

Figure 6. EXAFS fitting analysis. Comparison of the experimental (*) and theoretical (—) k^2-extracted EXAFS taken at the Cu K-edge of the $Cu_{1.00}V_2O_5$ ARG-like material using the fitting parameters as for the low level of doping metal. The sudden variation of the experimental spectrum at $k \sim 13.5$ is due to the presence of traces of zinc in the samples.

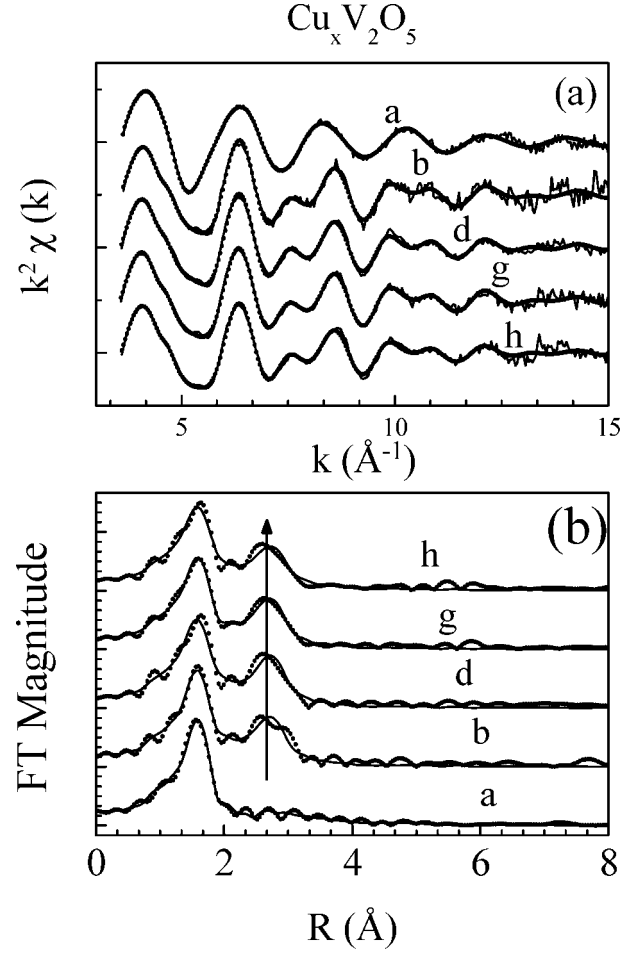

Figure 7. Best fit of the copper K-edge EXAFS signals of samples **a**, **b**, **d**, **g**, and **h**. The figure shows the comparison of the experimental (...) and theoretical (—) signals. Panel a displays the k-extracted EXAFS signals. The sudden variation of the experimental spectrum at $k \sim 13.5$ in sample **h** is due to the presence of traces of zinc in the samples. This interval has been excluded in the fitting procedures. Panel b shows the corresponding Fourier transforms, obtained in the 3.1–15 Å^{-1}, k space.

Figure 2a for a metal interaction with a single bilayer) that may be used as a fingerprint for the metal site location. In fact, when the inserted metal interacts within a single bilayer, the value of the angle M–O–V shown in Figure 2a is close to 100°. This occurs in chemically inserted $Zn_xV_2O_5$ and in low level of zinc- and copper-doped V_2O_5. This has been explored more fully by considering what the same angle would be when the inserted metal is placed between two bilayers. Looking at the Figure 1, it obviously approaches 180°. In this context, the experimental EXAFS signals would be strongly affected by a focusing effect[18] of the linear configuration M–O–V. Figure 5 shows the theoretical EXAFS signals computed ab initio on the M–O–V configuration (Cu in the calculation). The figure displays the total MS signal $\eta^{(3)}$ associated with the triplet Cu–O–V, computed

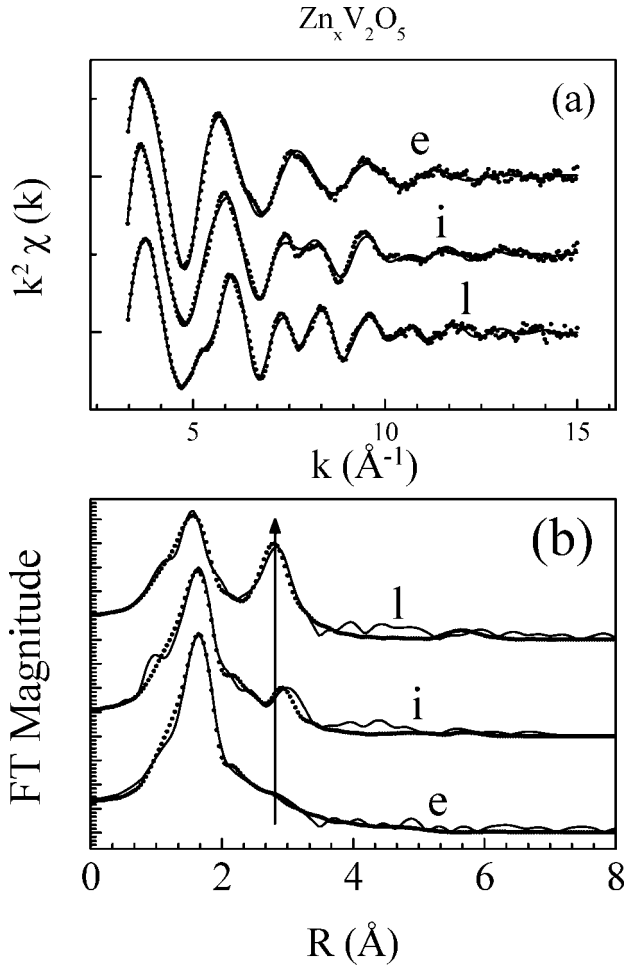

Figure 8. Best fit of the zinc K-edge EXAFS signals of samples **e**, **i**, and **l**. The figure shows the comparison of the experimental (...) and theoretical (—) signals. Panel a displays the *k*-extracted EXAFS signals. Panel b shows the corresponding Fourier transforms, obtained in the 3.1–15 Å^{-1}, *k* space.

considering linear (180°) or coplanar (100°) geometries of the triplet, that correspond to the "between two bilayer" or "single bilayer" interaction, respectively. It is worth pointing out that there is a dramatic increase of the signal due to the focusing effect in the coplanar case. This feature may be used as a fingerprint for the metal site location: the existence of the strong effect would modify the EXAFS spectrum of the metal K-edge, indicating that the metal is placed between two bilayers. On the contrary, EXAFS spectra of compounds where the metal interacts within a single bilayer would be characterized mainly by the first shell peak (M–O) and would be only slightly affected by the three-body contribution (M–O–V).

The fitting procedure was done using the atomic coordinates as shown in ref 12, and more detail is specified in the Experimental Section. First, in order to check the consistency of the present data analysis to the one already published,[12] the fitting procedure has been conducted with samples **a** and **e**. In light of the arguments that the structural model was that of Figure 2a, the following two-atom contributions have been included in the fitting procedure: $\gamma^{(2)}$ Zn_1–$O_{2,3,4,5}$ (first shell) with degeneracy of 4; : $\gamma^{(2)}$ Zn_1–$O_{12,13,14,15}$ (second shell) with degeneracy of 4. In addition, a three-body contribution, $\eta^{(3)}$ Zn–O–V, has been added as well. It takes into account the four triplets Zn_1–O_2–V_6, Zn_1–O_3–V_8, Zn_1–O_4–V_{10}, and Zn_1–O_5–V_{11}, and the notation $\eta^{(3)}$ includes both $\gamma^{(2)}$ Zn–V and $\gamma^{(3)}$ Zn–O–V. The overall number of parameters included in the fitting procedure was 12: 3 bond distances, 1 asymmetry coefficient β, 1 angle, 4 EXAFS Debye–Waller factors, and 3 nonstructural terms: E_0, S_0^2, and the experimental resolution. E_0 is displaced a few electronvolts from the edge inflection point.

The interatomic distances and the corresponding EXAFS Debye–Waller factors (best fit) of the samples investigated are shown in Tables 2 and 3 for both Cu and Zn K-edges, respectively. The statistical errors associated with the parameters obtained with the EXAFS analysis are also indicated, and they have with a 95% confidence interval. The latter were determined by correlation maps (contour plots) for each pair of parameters.[36] The comparison of the best fit parameters concerning samples **a** and **e** with literature data[12] confirm the consistency of the present data analysis. This is evident from the M–O first shell quotation in both set of data (Cu–O 1.960(5) Å and 1.970(6) Å; Zn–O 2.065(3) Å and 2.069(3) Å) as well as for the M–O–V angles involved (Cu–O–V 100(1)° and 101(1)°; Zn–O–V 96(1)° and 95(1)°.

In addition, from the signal point of view, an inclusion of the M–M interaction (Cu–Cu or Zn–Zn) was required when analyzing EXAFS data for high level doping metal samples. This is associated with a third two-body signal $\gamma^{(2)}$ Zn_1–$Zn_{7,9}$ with degeneracy of 2, which was included as demanded by the different fitting strategies. The necessity of including the M–M interaction in the fitting procedure of a particular stoichiometry is confirmed by Figure 6, which shows the comparison of the experimental and theoretical EXAFS signal for the highly doped sample **d**. The theoretical curve has been obtained considering only the signal used for the low-doped sample **a**. As may be see from the figure, the model fails even with parameter refining, and the residual curve (bottom) seems to be characterized by a well-defined sinusoidal signal, which is needed to be included. To determine the origin of the unaccounted signal and to find whether it related to the "between the bilayer" model, we compared the residual curve of Figure 6 with the theoretical signal of Figure 4. The two curves are found to be different in the position of the maximum, excluding any correlation of the residual signal to a possible Cu–O–V triplet. The EXAFS analysis confirms this suggestion, indicating that the Cu–Cu (or Zn–Zn) two-body signal corresponds to the residual curve of Figure 6, and hence its inclusion is required when analyzing EXAFS data of high doping level metal samples. Similar plots for samples **h** and **l** are reported as Supporting Information (Figures S1 and S2).

The best fit results are illustrated in Figures 7 and 8 for the Cu and Zn K-edges, respectively. Panel a of the figures shows the comparison of the experimental and theoretical curves of k^2-weighted EXAFS, and panel b displays the corresponding Fourier transform (FTs) compared. In the figures it is seen that the theoretical curves match well with the experimental ones in all panels, indicating the reliability of the chosen structural model and the accuracy of the data

(36) Filipponi, A. *J. Phys.: Condens. Matter* **1995**, *7*, 9343.

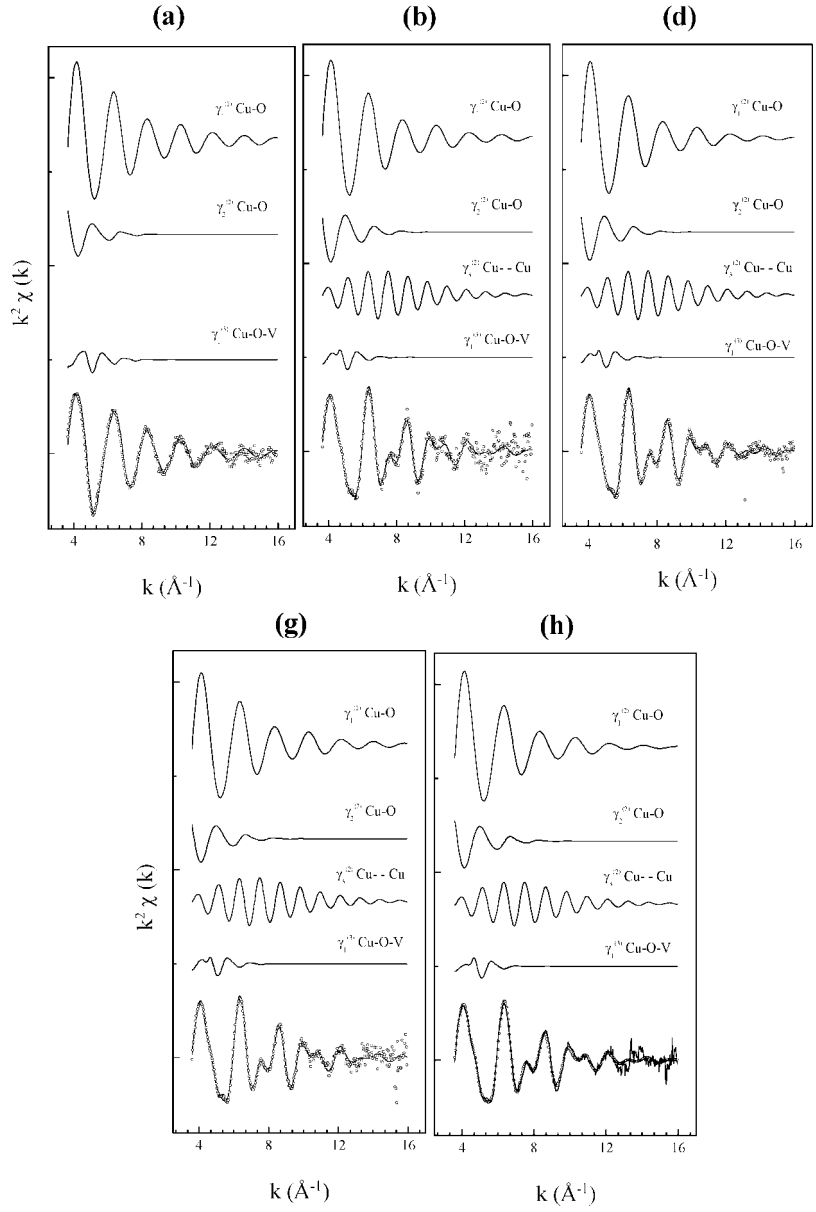

Figure 9. Details of the EXAFS analysis of the Cu K-edge of samples **a**, **b**, **d**, **g**, and **h**. Each panel of the figure shows the individual EXAFS contributions, in terms of two-body and three-body signals, to the total theoretical signal. At the bottom, the comparison of the total theoretical signal (—) with the experimental (...) is also illustrated.

analysis. A close inspection of the curves reveals changes at both EXAFS and FT signals of the two sets of data. In fact, the EXAFS signals displayed in panel a of both figures show modifications at about $k \sim 8$ and 11 $Å^{-1}$ (see also Figure S3 in the Supporting Information for a superposed EXAFS spectrum), and the FT magnitude of the second peak (at ~2.5 Å) of panel b (both figures) increases as the doping metal concentration increases. This is indicated by an arrow in the figures. The behavior indicates structural modification occurring in the outer shell, i.e., where the effect of the increased concentration of the doping metal makes visible metal–metal (Cu–Cu in this case) effects in the X-ray absorption spectrum. It is important to remark that the first shell of atoms are not concerned, and thus the sites where the metal ions are placed are not influenced by the metal concentration nor do experiments support the formation of a new (or second) site for the metal ion.

Figure 9 reports the details of the EXAFS analysis for the copper-doped samples. Each panel of the figure shows the various contributions to the theoretical signal and the comparison of the theoretical signal with the experimental one. First, the experimental signals are well reproduced in all panels, again pointing out the accuracy of the data analysis. In addition, besides the fact that the Cu–O first shell largely contributes in all panels, the two-body $\gamma^{(2)}$ Cu--Cu signal is very important and modulates all the EXAFS spectrum in samples **b** to **h**. The inclusion of this contribution in the fitting procedure of samples **a** and **e** did not improve the data analysis, leading to no improvement in fitting (structural parameters indicated in italics in Tables 2 and 3). It is also interesting to note that this $\gamma^{(2)}$ Cu--Cu contribution is shaped differently from the $\eta^{(3)}$ Cu–O–V, even when considering the high angle (180°, available in Figure 5). This is evident from a comparison of the $\gamma^{(2)}$ Cu--

Cu signal of Figure 9 with the $\eta^{(3)}$ Cu–O–V of Figure 5, i.e., the signals associated with the two models for the copper (metal) site for high level of doping samples. Once again, the data analysis supports the "one bilayer interaction" model of the site.

From the structural parameters indicated in Tables 2 and 3, the preferred site for both Cu and Zn at different metal concentrations is similar, with, for instance, the copper site to be 4-fold-coordinated by four oxygens at a distance of about 1.95–1.97 Å. The oxygens belong to the same V_2O_5 bilayer, and the metal is in a quasi-coplanar position with them, corresponding to an angle of about 100°. Zinc occupies the same site as found for copper. The Zn–O bond length for the first shell increases with respect to copper, leading to a value of 2.05–2.07 Å in the various samples. Generally, we have also seen that increasing of the level of metal doping produces an increased structural disorder. This is particularly evident while analyzing the EXAFS bond variances of the Cu–O and Zn–O first shell as well as the numerical values of the asymmetric parameter β, which are both seen to increase upon progressive metal insertion. Also in both series of data, the higher the doping level, the larger the M–O–V angle.

EXAFS at the Vanadium K-Edges. The EXAFS spectra taken at the vanadium K-edges have been studied as well. Generally, as emphasized several times in the literature,[13,30,31] the K-threshold of vanadium works as an excellent indicator of both charge and symmetry in V_2O_5 gel materials, and hence XANES spectra are analyzed first. Indeed, XANES spectra in Figure 3 indicate no significant difference in the vanadium atomic environment, apart from splitting of feature A in highly doped samples. This suggests that the vanadium site is only slightly affected by the insertion of a doping metal.

Because of the "characteristic" large asymmetry of the vanadium environment for the distances in the first shell, the EXAFS spectrum of a V_2O_5 gel is not a simple case for analysis, and a technique based on the natural polarization of synchrotron radiation beam was previously used[9,13] to solve this problem. This further improved by including analysis on powder samples.[12,15] Hereafter in the analysis we take advantage of using the same fitting approach, which is basically characterized by a constrained fitting procedure, allowing the structural parameters to float only within some limits, in agreement with those normally quoted for V_2O_5 gel compounds. This supports the reliability of the present EXAFS analysis, even considering the relatively large number of two-body contributions related to the V–O first shell. The approach was validated by the consistency of the polarized-powder measurements and data analysis.[15]

Figure 10 shows the comparison of the theoretical and experimental EXAFS spectra (panel a) of some copper- and zinc-doped samples and the corresponding Fourier transforms (panel b). From the plots it is seen that the theoretical curves match well with the experimental ones. EXAFS signals and the corresponding FTs of the low doped samples **a** and **e** are clearly the same. A comparison of the EXAFS signals related to samples of different metal level reveals slight differences in the spectra shape, and the FT curves are

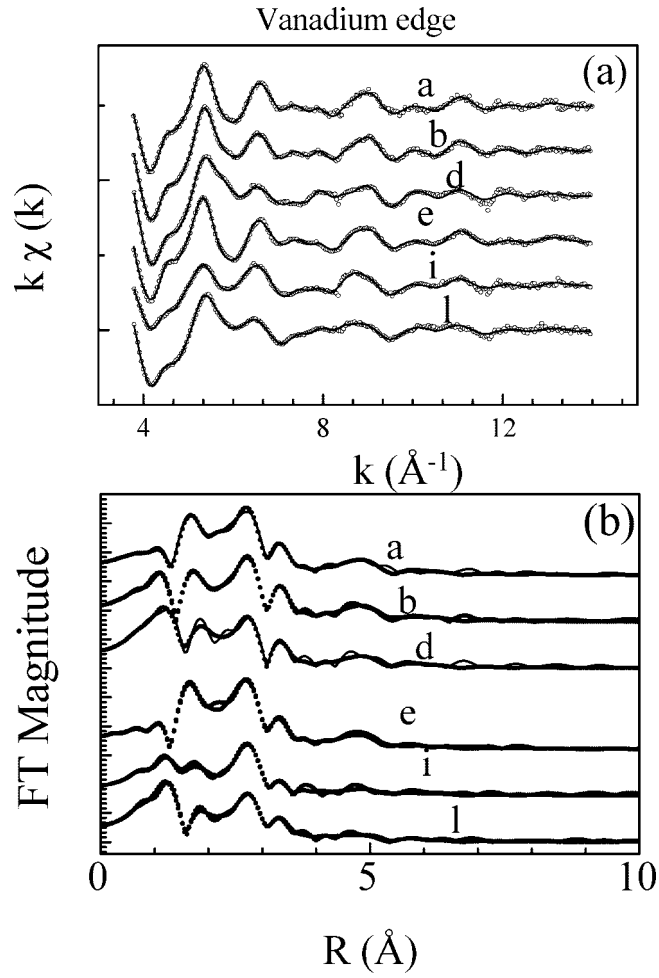

Figure 10. Best fit of the vanadium edge EXAFS signals of samples **a**, **b**, **d**, **e**, **i**, and **l**. The figure shows the comparison of the experimental (...) and theoretical (—) signals. Panel a displays the *k*-extracted EXAFS signals. Panel b shows the corresponding Fourier transforms, obtained in the 3.5–12 $Å^{-1}$, *k* space.

subsequently modified in their relative peak intensities. This behavior suggests local structure changes accompanied by effects of local structure disorder. In particular, the inclusion of the possible Cu (Zn)--V interactions seems to be required for samples of high levels of doping. It is worth noting that for the first time we have observed effects due to the presence of a doping metal that extend over the vanadium edge, in doped based V_2O_5 materials.

EXAFS analysis has been conducted, as is customary, that includes all the important MS paths of the fitting approach specified above and available in ref 12. Here, the standard signal was used to fit V_2O_5-based materials (5 $\gamma^{(2)}$ signals due to the vanadium first shell, 4 $\gamma^{(2)}$V--V signal generated by the vanadium in the second and third shell, and the three-body $\eta^{(3)}$ due to the V–O–V triplet) we have included the three-body $\eta^{(3)}$ due to the Cu(Zn)–O–V triplet which is due to the presence of the doping metal in highly doped samples. The signals also take into account the Cu(Zn)--V distance of the triplet Cu(Zn)–O–V. The fitting procedure was computed with 23 free parameters: 9 distances, 1 angle, and 10 Debye–Waller like factors. The other three parameters were E_0, S_0^2, and the experimental resolution. In the present discussion, the actual number of free parameters is lower because of the structural constraints mentioned above.

Table 4. Selected EXAFS Best-Fitting Results at the Vanadium K-Edge[a]

bond length [degeneracy] Debye–Waller	$x = 0.25$ Cu arg-like	$x = 0.50$ Cu arg-like	$x = 1.00$ Cu arg-like	$x = 0.50$ Cu xerogel	$x = 1.00$ Cu xerogel	$x = 0.25$ Zn arg-like	$x = 0.75$ Zn xerogel	$x = 1.00$ Zn xerogel
V–O apical "up"/Å (1)	1.61(2)	1.61(1)	1.62(2)	1.60(1)	1.60(2)	1.63(2)	1.62(2)	1.64(2)
σ^2/Å^2	0.006(2)	0.005(2)	0.006(2)	0.008(2)	0.023(10)	0.004(2)	0.003(2)	0.004(2)
V–O plane/Å (1)	1.71(2)	1.72(2)	1.71(2)	1.73(3)	1.71(2)	1.74(2)	1.70(2)	1.71(2)
σ^2/Å^2	0.010(7)	0.009(1)	0.012(8)	0.008(3)	0.005(2)	0.03(1)	0.023(10)	0.015(9)
V–O plane/Å (2)	1.91(2)	1.91(1)	1.91(2)	1.89(2)	1.91(2)	1.91(2)	1.92(2)	1.93(2)
σ^2/Å^2	0.005(2)	0.007(3)	0.012(8)	0.008(3)	0.02(1)	0.005(3)	0.012(8)	0.012(6)
V–O plane/Å (1)	2.01(4)	2.01(5)	2.03(4)	2.01(4)	2.00(3)	2.04(3)	2.00(2)	1.98(2)
σ^2/Å^2	0.03(1)	0.02(1)	0.03(1)	0.03(1)	0.03(2)	0.03(2)	0.009(7)	0.03(2)
V–O apical "down"/ Å (1)	2.35(4)	2.32(4)	2.33(4)	2.30(4)	2.35(4)	2.38(3)	2.341(4)	2.34(4)
σ^2/Å^2	0.03(1)	0.02(1)	0.02(1)	0.026(10)	0.013(10)	0.02(1)	0.009(6)	0.010(6)
V–O–V/deg (2)	154(4)	152(3)	150(4)	153(3)	155(4)	154(2)	152(3)	153(3)
$\sigma^2\theta$/deg^2	21(6)	18(10)	27(8)	65(20)	45(10)	68(15)	31(10)	24(12)
V--V/Å[b]	3.53	3.55	3.53	3.52	3.53	3.57	3.52	3.54
V–O–Cu(Zn)/deg		104(4)	106(4)	106(6)	109(3)		99(3)	103(3)
$\sigma^2\theta$/deg^2		77(30)	75(20)	79(40)	59(20)		67(30)	79(25)
CN		2.5(5)	2.4(5)	1.5(4)	2.4(5)		2.4(4)	1.5(4)
Cu(Zn)–O/Å		1.95(5)	1.97(7)	1.97(6)	1.99(6)		2.03(6)	2.07(5)
σ^2/Å^2		0.02(1)	0.010(6)	0.009(3)	0.009(4)		0.009(3)	0.014(9)
V--Cu(Zn)/Å[b]		2.81	2.88	2.85	2.95		2.78	2.95

[a] Data are in Å. The estimated parameter errors are indicated in parentheses. [b] Data obtained from the three body configuration (using angle M–O–V and distances V–O).

Table 4 reports a selection of the best-fit results (interatomic distances and the corresponding EXAFS Debye–Waller factors) at the vanadium K-edges. The errors associated with the parameters obtained with the EXAFS analysis are indicated as well. Looking at the bond length of the VO_6 octahedron, we confirm that the symmetry around the vanadium site does not change much for the various samples. The doping metal only slightly modifies the distances, with variations in the order of few (1–3) hundredths of an angstrom. The associated EXAFS bond variances change differently, and the xerogel materials are more ordered than the aerogel-like materials. At this edge, the specific parameters associated with the copper (or zinc)–vanadium interaction is the angle V–O–Cu(Zn), which is found to be in the 99°−109° range and which is seen to increase as more copper (zinc) is inserted in the gel. The other parameters are the O–Cu and the V–O apical "up" bond distances. As seen from the metal edges, the O–Cu bond length are shorter than the O–Zn first shell. In addition, using the numerical value of Table 4, the V--Cu (or V--Zn) interactions are determined by geometry and ranging from 2.81 Å (low stoichiometry) to 2.95 Å (high stoichiometry).

As the doping ions are distributed through the material, the new atomic interactions seen are the Cu–O–V (or Zn–O–V) triplets. These atomic configuration can be described simply by two distances and one angle. The distances are (for the copper case) the O–Cu and the V–O apical "up". The angle is the V–O–Cu. These interactions are shown by both metal sites investigated, i.e., copper and vanadium. Of course, the two sets of independent data should be consistent. The strength and limitation of this approach could be revealed by a comparison of Tables 2, 3, and 4. The angles of the triplet Cu–O–V are found constant when studied for both copper and vanadium, and hence the two sets of data are consistent. The same is also true for the zinc case. In addition, it is observed generally that the insertion of the metal ions produces a progressive increase of the corresponding angles. Referring to the Cu–O (or Zn–O) first shell distances, we conclude that the data are consistent, though the better determination of the distances (considering the associated errors, in parenthesis of Table 4) are yielded from analysis of the copper (zinc) K-edge. This is not surprisingly since, at the Cu K-edge, the Cu–O interaction is the first-shell contribution.

Conclusions

The insertion chemistry characteristic of gel-based V_2O_5 materials serve as host materials for Li^+ ions as well as for polyvalent cations. The present work highlights the importance of the XAS technique to study the site and the local structure of selected atoms in an amorphous structure. A complete understanding of the metal ion intercalation onto V_2O_5 gels has been provided and reveals the preferred site for the doping metal ion.

The EXAFS analysis shows that the vanadium atomic environment is not altered by the doping metal insertion and that the doping metals (Cu and Zn) are found to occupy the same site. Copper and zinc are 4-fold-coordinated by almost coplanar oxygens. This suggests a preferred site for the doping metal (M) and the same interaction between the vanadium and the doping metals. The preferred site where the metal ions are located remains the same over the full range of doping level, from $x \sim 0.25$ to $x \sim 1.0$. The number of equivalent sites available to the doping metal in the bilayer V_2O_5 structure would be filled when $x = 1$. This, in turn, means that for the high concentration samples the M–M interaction should appear at distances of about 3–3.2 Å. Both metal K-edges analyzed in the investigated compound of high stoichiometry proved that the EXAFS contribution of the M–M interaction is observed. In fact, when the metal doping level is increased above 0.25, the M–M contribution becomes progressively more significant, and its inclusion is required in the fitting procedure. This contribution must also be taken into account when analyzing the vanadium K-edge. The two sets of independent data are consistent, although metal

K-edges are favored in the determination of the M–O first-shell bond length.

The V K-edge XANES spectra indicated no significant differences in the vanadium atomic environment for the studied compound or in the case of the same material made by two different routes of synthesis. XANES at the metal K-edges are shaped similarly. Also, no shift of the edge in both series of spectra, within the experimental resolution, is detected as the metal level content increases.

When the doping ions interact with a single bilayer, an important consequence is that the interlayer space is free and available for further ion insertion. This could be an explanation for the excellent reversible insertion of lithium ions into the doped structure. For example, $Cu_{0.1}V_2O_5$ xerogel cathodes were able to deliver 180 mAh/g in 80 min and discharge for more than 450 cycles[4] without any capacity fading. These excellent properties could be related to the "free" space.

Acknowledgment. We appreciate the support of DOE under contract DE-FG02-01ER15221. Measurements at Daresbury Laboratory were supported by the European Community-Research Infrastructure Action under the FP6 "Structuring the European Research Area" Programme (through the Integrated Infrastructure Initiative "Integrating Activity on Synchrotron and Free Electron Laser Science").

Supporting Information Available: EXAFS fitting analysis using old model at the Cu K-edge, EXAFS fitting analysis at the Zn and V K-edges, and XRD pattern. This information is available free of charge via the Internet at http://pubs.acs.org.

CM701910C